Hydrology and
Earth System
Sciences
Discussions

Open Access

EGU

Evaporation from Savanna and Agriculture in Semi-Arid West Africa

Natalie C. Ceperley[1,2], Theophile Mande[2], Nick van de Giesen[3], Scott Tyler[4], Hamma Yacouba[5], Marc B. Parlange[1,2]

5 [1]Department of Civil Engineering, Faculty of Applied Sciences, University of British Columbia, Vancouver, British Columbia, V6T 1Z4,Canada

[2]Laboratory of Environmental Fluid Mechanics and Hydrology, School of Architecture, Civil and Environmental Engineering, Swiss Federal Institute of Technology, Lausanne, 1015, Switzerland

3Department of Civil Engineering and Geosciences, Delft University of Technology, 2600 AA, Delft, Netherlands

10 [4]Department of Geological Sciences & Engineering, University of Nevada, Reno, Nevada, 89557, United States of America

[5]Laboratory Hydrology and Resources in Water, International Institute for Water and Environmental Engineering (2iE), Ouagadougou, 01, Burkina Faso

Correspondence to: Natalie C. Ceperley (natalie.ceperley@unil.ch)

15 **Abstract.** Rain-fed farming is the primary livelihood of semi-arid West Africa. Changes in land cover have the potential to affect precipitation, the critical resource for production. Turbulent flux measurements from two eddy-covariance towers and additional observations from a dense network of small, wireless meteorological stations combine to relate land cover (savanna forest and agriculture) to evaporation in a small (3.5 km^2) catchment in Burkina Faso, West Africa. We observe larger sensible and latent heat fluxes over the savanna-forest in the headwater area relative to the agricultural section of the

20 watershed. Fluxes above the savanna-forest are higher because of the greater number of exposed rocks and trees and the higher productivity of the forest compared to rainfed, hand-farmed agricultural fields. We deduce that there is a higher soil heat flux in the fields. Vegetation cover and soil moisture are found to be the primary controls of the evaporative fraction, defined as the latent heat over the available energy. Satellite derived vegetation index (NDVI) and soil moisture are determined to be good predictors of evaporative fraction. Our measurements provide an estimator that can be used to

25 estimate evaporative fraction when only NDVI is available. Such large-scale estimates of evaporative fraction from remotely sensed data are valuable where ground-based measurements are lacking, which is the case across the African continent and many other semi-arid areas. Evaporative fraction estimates can be combined, for example, with sensible heat from measurements of temperature variance, to provide an estimate of evaporation when only minimal meteorological measurements are available in remote regions of the world. These findings reinforce local cultural beliefs of the importance

30 of forest fragments for climate regulation and may provide support to local decision makers and rural farmers in the maintenance of the forest areas.

Hydrology and
Earth System
Sciences

Open Access

EGU

Discussions

1 Introduction

The sudanian savanna in South-Eastern Burkina Faso is a patchwork of savanna, forest, and scrubland. Vegetation is mainly deciduous according to the seasonal cycle of moisture availability, but spatial variations in topography and water availability result in different seasonal patterns according to land cover. Historically, people in this region rely on a mix of hunting and

5 gathering, small scale agriculture, and pastoralism. As land claims and regulations have changed, communities have been forced to rely more on agricultural production as a primary source of food and income, resulting in land conversion for agriculture. Today small-scale rain fed agriculture is the dominant livelihood in large parts of West Africa, despite its high level of dependence on seasonally controlled hydrology. Conversion of the landscape to agriculture involves removing rocks, trees, natural grasses, and tilling the soil (Swanson, 1978). Transformation of forestland to agriculture has been shown

10 by model simulations to alter global circulation, hydrology, and biogeochemistry both in the present and in predictions of the future (Abiodun et al., 2008; Feddema et al., 2005; Mande et al., 2011; Steiner et al., 2009; Sylla et al., 2015; Vitousek, 1997).

Modification of the land surface results in changes to the physical environment, and specifically hydrological fluxes, by altering the components of the surface energy budget (Pielke et al., 2002). The partition of net radiation into sensible heat,

15 evaporation, and soil heat flux drives global atmospheric processes and is controlled by interacting surface and atmospheric conditions (Foken, 2008; Szilagyi and Parlange, 1999). The surface energy budget is written Eq. (1):

$$R_n = L_e E + H + G, \text{ (1)}$$

where $L_e E$ is latent energy flux, H is sensible heat flux, R_n is the net radiation, and G is the soil heat flux.

The sensible heat, Eq. (2):

20 $$H = \rho c_p \overline{w'T'}, \text{ (2)}$$

and latent heat, Eq. (3):

$$L_e = L_e \rho \overline{w'q'}, \text{ (3)}$$

fluxes can be obtained from eddy covariance and the using the above equations, where ρ is the air density, c_p is the specific heat, $\overline{w'T'}$ is the covariance of fluctuations of vertical wind speed and temperature, L_e is the latent energy of vaporization,

25 and $\overline{w'q'}$ is covariance of fluctuations of vertical wind speed and humidity.

The energy balance is challenging to close even in areas and regions with extensive datasets and accessibility, and is particularly challenging in areas with complex surfaces (Burba, 2013; Domingo et al., 2011; Farhadi, 2012; Federer et al., 2003; Foken et al., 2009; GUO et al., 2006; Katul and Parlange, 1992; Krishnan et al., 2012, 2012; Kustas et al., 1994; Parlange and Katul, 1992; Williams et al., 2012). Evaporation from vegetated surfaces remains the component of the global

30 distribution of water that is the least frequently measured and thus the least well understood (Brutsaert, 1982; Brutsaert and Parlange, 1992; Burba, 2005; Compaore, 2006; Crago, 1996; Crago and Qualls, 2013), particularly in West Africa, due to limited field observations (Bagayoko et al., 2007; Dolman et al., 1997; Gash et al., 1997; Mande et al., 2011). A connection

exists between changes in albedo and the occurrence of drought in West Africa, although the physical processes and direct implications for desertification are debatable (Charney, 1975; Nicholson et al., 1998).

The evaporative fraction, the ratio of latent heat to available energy, is useful to estimate total daily evaporation with measurements of a single component of the energy balance and to up-scale surface measurements using remote sensing

5   products (Brutsaert and Sugita, 1992; Compaore, 2006; Porte-Agel et al., 2000; Shuttleworth, 1989; Szilagyi et al., 1998; Szilagyi and Parlange, 1999). Evaporative fraction is based on the concept of self-preservation in the diurnal evolution of the surface energy budget (Brutsaert and Sugita, 1992; Porte-Agel et al., 2000), stating that the diurnal cycle each of the energetic fluxes will resemble that of available energy, even if there is variation in the quantity, allowing for exploiting satellite data that are typically only obtainable once a day at best. Remotely sensed land surface temperature is currently the

10   primary tool for mapping the surface energy budget over a large area (Bateni and Entekhabi, 2012). Evaporative fraction is constant during day time in fair weather conditions (Gentine et al., 2007) but can be much less constant when moisture circulation rates are high and available soil moisture increases (Lhomme and Elguero, 1999). Seasonal progression of evaporative fraction responds faster to rainfall and moisture availability in grassland than in woodland, and variations are not explained by meteorological conditions, including cloudiness alone, but rather change in surface resistance and moisture

15   advection and availability (Farah et al., 2004).

We measured the complete energetic and hydrologic fluxes in two sites of a semi-arid, mixed-use catchment over a year and a half, capturing both the greening and dry-down phases. The land is used as a agroforestry parkland farmed every 2-3 years and a forested area made up of evergreen trees arranged in a gallery forest surrounding a spring and an open wooded savanna (savanna-forest) on a raised plateau. These land covers are representative of the surrounding region and capture the range

20   from more to less anthropogenic land uses. The multi-use comparison over multiple seasonal cycles makes this study unique (Bagayoko et al., 2007; Ezzahar et al., 2009; Guyot et al., 2009; Mauder et al., 2006). We calculate the evaporative fraction over the study period and compare it with land cover and atmospheric controls. Our measurements are significant because they allow calibration and comparison for calculation of the components of the energy budget from lower cost and more easily maintained stations (Nadeau et al., 2009; Simoni et al., 2011) and corresponding data from satellite imagery. This

25   study has implications for development priorities, as it takes place in context where local livelihood can be dramatically affected by slight changes in the water balance and land cover. Our results point to the necessity for ground measurements for eventual up-scaling from point to regional evaporation measurements in remote and less-studied regions of the globe. We began this work with discussion with community partners and to bring it full circle we conclude this paper by relating it back to the cultural context.

2 Measurements and Calculations

2.1 Site Description

Observations were made in small catchment (3.5 km^2 area) neighboring the village of Tambarga in the commune of Madjoari, in the Gourma Province, in Burkina Faso, West Africa (figure 1). The ephemeral stream defining the catchment
5 (outlet is 11°26'29.7"N 1°12'57.7"E) flows into the Singou River, which joins the Pendjari River and eventually flows into the White Volta of the Volta River Basin, the third largest river basin by area in West Africa, after the Niger and the Senegal. A rocky escarpment defines the catchment with a plateau on average some 100 meters above the lower agricultural fields and the soil is predominantly sandy-loam (Ceperley, 2014). These fields are the "house" farms and are smaller than the main economic farms. In 2009, they were farmed with short rotation millet and in 2010 they were left fallow. Plowing
10 occasionally uses animal-drawn plows, but is primarily done by hand – this is not intensive agriculture. The open wooded savanna (savanna-forest) on top of the rocky escarpment and rain-fed grain (corn or millet) are the two dominant land covers of the catchment according to area. At opposite ends of the catchment, there is a dense gallery forest in the valley that grows near permanent springs and an ephemeral wetland used for rice cultivation near the point considered the outlet of the watershed. Farming is the main livelihood in the village and crops include millet, sorghum, cotton, and rice. Agroforestry
15 trees in the fields are common and consist most often of the tree species *Vitellaria paradoxa*, *Sclerocarya birrea*, and *Ficus* sp. (Bordes, 2010). The village is made up of a majority of people from the Gourmantche ethnic group, though there is a significant population of Peulh, and some migrants of other areas of Burkina Faso or neighboring countries.

The watershed falls in the sudanian climatic zone, defined by alternating wet and dry seasons, with the rain falling between May and September. The natural vegetation is sudanian-wooded savanna, composed of a mix of deciduous woody trees,
20 shrubs, and tall grasses. In addition, due to the variation in topography and water availability, there are gallery forests near streams or rivers that contain many species endemic further south, Guinean zone. The surrounding area is a patchwork of hunting reserves and national parks, and thus has a higher level of vegetation cover than most of the country. This watershed is a prime location to study the consequences of land use change from sudanian savanna to agricultural fields, since it contains both open wooded savanna that hasn't been memorably farmed and regularly farmed fields. Agriculture is primarily
25 rainfed and not mechanized corn and millet cultivation. In addition, the surrounding sudanian savanna, which is characterized by fire-selected grasses ranging from 20 centimeters to 1.5 meters in height also includes patches of woody scrub-land, open forests, gallery forests, and riparian stands (Arbonnier, 2004).

2.2 Field Measurements

Two energy balance stations were installed from May 2009 through September 2010. One was situated in an agricultural
30 field planted with short season millet in 2009 and left fallow in 2010, and the second one measured over the gallery forest when the wind came from the West (90°±45°) and over the open wooded savanna when the wind came from the South (180°±45°). They were equipped with sonic anemometers, gas analyzers, net radiometers, and air temperature and humidity

Hydrology and
Earth System
Sciences

Open Access

EGU

Discussions

sensors (table 1). Eddy-correlation equipment was placed facing two opposite directions (46º and 226º) on the lower station over the field and in the dominant wind direction on the upper station over the gallery forest. Nearby the station in the field was a high precision rain gauge measuring at a resolution of 0.1 mm. In addition, a network of up to 12 small meteorological stations (Ingelrest et al., 2010), was distributed across the watershed with sensors to measure incoming solar radiation, wind

5   direction and speed, air temperature and relative humidity, rainfall, soil moisture and temperature, and surface temperature. In this analysis, we use data from May 2009 - October 2010, the 15 months with both towers operational, but when possible, we present the longest time series possible for climatic context. We attempted to measure ground heat flux using heat flux plates but ultimately rejected the observations because of irregularities in the land surrounding the plates.

2.3 Flux Calculation

10   The fluxes of sensible (H) and latent (L_eE) heat were measured at a half hour time step. Only day light measurements, consistently between sunrise and sunset (8 am - 4 pm), corresponding to when energetic fluxes were of significant magnitude, were used for the comparison. The total available energy, H + L_eE, was subtracted from the net radiation, R_n, to give an indicator of ground heat flux (G, see equation 1), any unaccounted for flux transfers, and the error (Brutsaert, 1982; Higgins, 2012).

15   We used a planar fit correction that effectively tilted measurements of the three components of the wind field perpendicular to the direction of flow, so that the vertical wind was equal to zero over one month averaging periods (Aubinet et al., 2012; Burba, 2005; Oldroyd et al., 2015; Rebmann et al., 2012; Wilczak et al., 2001). We then performed a linear regression using the mean wind vectors to obtain a matrix that we used to adjust wind vectors and stress tensors in a new coordinate system with a z-axis perpendicular to the mean streamline. Finally, we rotated the intermediate winds and stress tensors. The Webb-

20   Pearman-Leuning equation (Foken et al., 2012; Leuning, 2007; Webb et al., 1980) Eq. (4):

$$E = (1 + \mu\sigma)\left(\overline{\omega'\rho'_v}\right) + \frac{\overline{T}}{\rho_v}\overline{\omega'T'}. \quad (4)$$

was used to correct for any influence of trace gas concentrations on temperature and humidity fluctuations.

2.4 Evaporative Fraction

Evaporative fraction (EF) was calculated for each half hour of data, separately over the savanna-forest and the agricultural
25   area by dividing the latent energy by the available energy defined by the sum of sensible and latent heat flux. The midday average (10 am - 2 pm) was used as the EF for a given day as that is when it was the most stable over the year (figure 5) Eq. (5):

$$Ef = \frac{L_eE}{H + L_eE}. \quad (5)$$

2.5 Volumetric Water Content

Volumetric water content (VWC) in the soil was monitored at 15 and 30 cm depths in 2009 and at 5 and 20 cm depths thereafter at some of the small meteorological stations representative of the various land covers (Table 1) using a measure of soil dielectric permittivity and converted to VWC (Topp et al., 1980). Measurements were averaged on the half hour time

5   step for comparison with EC measurements and by day for comparison with EF. Gaps in measurement were due to sensor malfunction. A vertical, spatial average of measurements at various depths was used to obtain a continuous record for the watershed.

2.6 Cloud Cover

Cloud cover was calculated by dividing the incoming shortwave infrared radiation measured with a radiometer (table 1) at

10 each small meteorological station by the theoretical incoming radiation calculated with a simple model (Whiteman and Allwine, 1986) for each of the small meteorological stations operating on any given day Eq. (6):

$$CC = \frac{sw_{measured}}{sw_{Whitman\&Allwine}}. \quad (6)$$

The cloud cover was calculated independently for all stations and then averaged to give a single value per day.

2.7 Vegetation Index

15 Normalized difference vegetation index (NDVI) is based on the amount of infrared radiation absorbed, which is related to the amount of photosynthesis taking place. It is considered a measure of the density of chlorophyll. NDVI is a ratio of the near infra-red (NIR) to red wavelengths Eq. (7):

$$NDVI = \frac{NIR - Red}{NIR + Red}. \quad (7)$$

Seasonal change in NDVI was observed by extraction of the area of interest from the 250-meter resolution West Africa

20 eMODIS 10-day temporally smoothed data (USGS FEWS NET). It has been corrected for molecular scattering, ozone absorption, and aerosols and then smoothed using a least square linear regression (Swets et al., 1999). The NDVI values are validated with *in situ* observation and photographs. The pixels that contained our stations were extracted to give a catchment – wide seasonal impression of the vegetation change.

2.8 Net Radiation

25 To account for any scale discrepancies between the small meteorological stations and the energy balance stations, net radiation was calculated at each small station (Brutsaert, 1982). Net shortwave radiation was calculated using the measured incoming shortwave radiation (table 1) and albedo (α) Eq. (8):

$$sw_n = (1 - \alpha) \cdot sw_i. \quad (8)$$

Albedo was measured using solar radiometers facing up and down for 155 days between October 2011 and November 2012.

30 Since albedo is heavily correlated with soil moisture and vegetation cover, a linear regression model of albedo based on soil

moisture and NDVI was used to estimate albedo when it was not measured. When either soil moisture or NDVI was not available, a linear model based just on the other, available metric was used. Gaps were filled with a linear interpolation and data missing at the beginning of the observation were filled using a linear interpolation based on average albedo for the day of the year (between April 22-25, 2009). All estimate albedo values were smooth using a 10-day moving average filter.

5   Albedo fell within the acceptable range for the vegetation covers (Figure 2). Long wave radiation was calculated as the sum of long wave upwelling radiation, Eq. (9):

$$Rl_u = \varepsilon_s \sigma T_s^4 \ . \ (9)$$

where ε_s is the surface emissivity, taken to have an average value (0.97), σ is the Stefan Boltzmann constant, and T s is the measured surface temperature, and the incoming long wave radiation, which is taken as a fraction of clear sky incoming long

10   wave radiation, Eq. (10):

$$Rl_i = Rl_{ic}(1 + am_c^b), \ (10)$$

where Eq. (11):

$$Rl_{ic} = \varepsilon_{ac} \sigma T_a^4 \ . \ (11)$$

and m_c is the measured cloud cover (6), a and b are constants, ε_{ac} is the atmospheric emissivity during clear sky conditions,

15   and T_a is the measured air temperature. The atmospheric emissivity is Eq. (12):

$$\varepsilon_{ac} = a'(\frac{e_a}{T_a})^{\frac{1}{7}} \ . \ (12)$$

where e_a is the vapor pressure near the surface, determined with the measured relative humidity and air temperature and a' is calculated with a Beta function and air temperature and averages 1.24 at our site as it does for average meteorological conditions (Brutsaert, 1982). Comparison to the measured net radiation at the energy balance station (figure 3) shows some

20   discrepancies. These may be due to the difference in wave lengths measured by the solar radiation sensors at the small meteorological stations, which use a silicon photodiode detector to detect radiation at wavelengths of 300 to 1100 nanometers. Whereas the pyranometer measures from 300 to 2800 nm and the pyrogeometer from 4.5 to 42 µm. The spectral response of the individual sensors was not available at this time, but estimation using standard spectra (ASTM G173-03 Reference Spectra) integrated over the two different short wave ranges indicates that the solar radiation sensors measure

25   61.78% of the energy that the pyranometers measure. These differences would be further exaggerated by the geometry of the sensor (180° for sw$_i$ and 150° for sw$_u$ from the pyranometer versus the solar radiation sensor which is less than 100% for the full 180°) especially in dusk and dawn conditions. Additionally, the effect of albedo varies according to cloudiness and sun altitude. Most of the radiation emitted by the earth and atmosphere is between 4 and 100 µm and measurements are often flawed because instruments themselves emit radiation of comparable wavelengths and intensity to the long wave radiation

30   that we want to measure. Thus our comparison is reasonable because it is of a similar order of magnitude, further fine-tuning the calculation will be done in a subsequent work.

Hydrology and
Earth System
Sciences

Discussions

Open Access

EGU

3 Results

3.1 Seasonality

A total of 1600 millimeters (mm) of precipitation was measured over the period of intensive monitoring, 2009-2010, 789
mm in 2009 and 811 mm in 2010 and it fell almost entirely during the period from May to October. As seen in figure 4,
5   average air monthly air temperature, cloud cover, soil moisture and NDVI followed the seasonal cycle of the rain:
temperature was higher in the dry season (November - March) than in the wet season (May - October); cloud cover was
lower in the dry season and increased starting in March and April peaking both years in July; soil moisture was highest in the
wet season; and vegetation, as shown by NDVI, increased over the course of the wet season, starting in May and peaking in
September and declining afterwards as grasses senesced. Separation between the lower and upper parts of the catchment is
10 apparent in the NDVI time series, where the savanna-forest consistently stays more green, with the field only surpassing it
due to its delayed senescence in September 2010. Plowing, early season harvests, and late season harvests are visible earlier
in some years over only the agricultural land. However, since these are averages over a few potentially mixed pixels, which
were composed of multiple crops, the individual behaviors are not visible. The land use differentiation is visible even at 250
m pixel resolution.

3.2 Components of Energy Balance

3.2.1 By day

The average diurnal cycle of the energy balance varied according to month (figure 5). In this figure, we compare a single day
in April with a single day in July. April is before the wet season begins, and prior to any vegetation growth in the agricultural
field, however, some of the evergreen forest canopy is already visible in the photos. By July, crops or fallow are growing in
20 the field and the canopy is greener. This change in vegetation cover and moisture availability is apparent in the diurnal
patterns of the energy balance for the both sizes. Net radiation is slightly higher during the wet season for both land covers,
and none of the fluxes are as consistent, which can be explained by the presence of atmospheric humidity and cloud cover.
The sensible heat is higher for both land covers in the dry season, however over the savanna-forest there is still latent flux
that nearly matches the sensible heat flux even in the dry season. By July, the latent heat flux has surpassed the sensible
25 heath for both land covers. Over the savanna-forest, we can see that the latent heat doesn't decline until the late afternoon,
suggesting that it is radiation limited and not moisture limited, whereas over the field it peaks closer to midday. The residual,
which is a combination of the ground heat flux and any error, is lower over the savanna-forest, and is negative in the
afternoon. The evaporative fraction is correspondingly higher in the rainy season than in the dry season and as we would
expect, has a higher value over the savanna-forest in the dry season but over the agricultural field in the wet season.
30 Net radiation was the most similar component between the two sites, although during the "dust" season of March and April,
it was lower over the savanna-forest. Sensible heat was greater over the savanna-forest for all months, with the greatest
difference in the "hot" period of March through May, which is an important period for the triggering of early convective

storms. Latent heat was also observed to be greater over the savanna-forest compared to the agricultural field. The timing of the peaks of latent energy signals when the system is moisture limited; during the early part of the year, the dry season through May, the diurnal cycle of latent energy peaked over the agricultural field during the mid morning, from 9 to 10 am, whereas over the savanna-forest, during the same period, the peak in the diurnal was after noon. Since latent energy flux has

5 a maximum daily value less than its absolute maximum, we know all moisture was depleted. In general, our data shows that latent energy flux was greatest at early in the diurnal cycle during the dry season, which suggests depletion of all available moisture early in the day. In contrast, during the rainy season, it declined, following the cycle of available radiation.

3.2.2 Over entire study period

There is high correlation for net radiation and a general correlation of total available energy (figure 6) between the savanna-
10 forest and the field, with more scatter occurring when soil was wetter (blue). There is more available energy over the savanna-forest than over the field, since there are equal amounts of net radiation, we can deduce that there is a greater ground heat flux in the field. The lack of shading below in the field, and the greater abundance of trees, with a high level of productivity, and rocks support this observation. Examination of the two components of net radiation - net long wave and net short wave - shows that soil moisture exerts much greater control on net long wave radiation, with the change in net long
15 wave radiation over the changes in soil moisture in the field much more apparent. Although there is more scatter in net shortwave when soil is wetter, it is less uniformly a response to the two land covers. The savanna-forest's net long wave radiation is greater when the soil is dry whereas the agricultural area has greater net long wave when it is wet. Sensible heat over all land covers is greater under dry conditions than wet (blue), but both sensible and latent energy flux are greater over the savanna-forest than the agricultural field regardless of soil moisture.

20 Division of the analysis according to wind sector revealed that certain features, for example over the ephemeral wetland and the gallery forest, contributed higher fluxes. There is a scale discrepancy between the eddy covariance measurements and the net radiometer measurements since the latter only senses exchanges directly above and below it whereas the former's range of detection can span a larger area depending on the wind speed. To account for this, we modeled the net radiation at each small station and then compared it to that measured with net radiometers with acceptable results (figure 3).

25 Further examination reveals that surface temperature and net long wave radiation have a strong negative correlation (figure 7) that is controlled by variations in soil moisture. Over the agricultural field, there is more scatter whereas over the savanna-forest, there is a minimal level of about -170 W/m2 for net long-wave radiation. This can be explained by the presence of the tree canopy that buffers the bare ground from the radiation loss (Figure 8).

3.2.3 Month by month

30 Figure 9 shows the two contrasting trends in surface heat fluxes by comparison of the month-by-month ratios between the measurements over the savanna-forest and agricultural land. The savanna-forest contributed more sensible and latent heat flux throughout the year (ratio < 1), but the difference in H between the two sites was greatest at the end of the year, the

beginning of the dry season, and the difference L_eE between the two sites was greatest at the beginning of the year, after land was cleared by burning. These trends were consistent over the two years of measurement, however there were some months (July and August 2010) when H was close to equal in the two sites. The higher level of similarity in H between the two sites in 2009 can be explained by the crop choice that year; That field was planted with early (60-95 day) maturing pearl millet

5   crop compared to its usual late variety (130-150 days), requiring a unusually late tilling and an unusually early harvesting, resulting in bare ground during the growing season. These differences are also visible in the NDVI (figure 4). Net radiation was more similar than the other fluxes; the greatest difference occurred when there is bare ground in the field, at end of the dry season, suggesting a higher albedo during this time.

3.3 Evaporative Fraction

10 #### 3.3.1 Correlations with surface and atmospheric conditions

Examination of the relationship between evaporation and the environmental variables that dominate in various models, shows that for our site, soil moisture and vegetation cover have the strongest positive correlation with evaporative fraction (figure 10). Over both the savanna-forest and the field, we see that landscape moisture availability, expressed as both NDVI and soil moisture (VWC), exert a strong influence on the evaporative fraction, with higher rates of evaporation occurring at

15 higher levels of soil moisture and vegetation cover, or in other words moisture availability from either plant or soil. Total net radiation does not show a strong influence, suggesting that this is not a radiation-limited system.

Wind speed shows a strong negative correlation with more evaporation occurring at lower wind speeds, contrary to standard evaporation models. Evaporative fraction and the cloud cover exhibit a positive correlation both over the field and the savanna-forest and could be explained by a two part discontinuous function, with a break at 0.4 (Brutsaert, 1982). In a

20 radiation limited system, cloud cover would reduce evaporative fraction, but in this case, since it is positive, we can deduce that cloud cover is an indicator of high rates of evaporation and moisture availability, thus further supporting our supposition that this is a moisture limited system.

3.3.2 Explanatory model

The relationship between soil moisture, vegetation index, and evaporative fraction can be fit with a linear regression (figure

25 11), Eq. (13):

$$\begin{cases} EF_{agriculture} = 0.41 \cdot NDVI + 1.4 \cdot VWC + 0.27 \\ EF_{Forest-Savana} = 0.48 \cdot NDVI + 0.35 \cdot VWC + 0.34 \end{cases} \text{(13)}$$

Evaporative fraction depends on both soil moisture and vegetation index over agriculture, whereas over the savanna-forest it responds more directly to vegetation index, as shown by the direction of the evaporative fraction color gradient. The evaporative fraction is more variable over the agricultural field, explaining the less good fit of the regression compared to

30 over the savanna-forest. Inclusion of net radiation, cloud cover, down-welling radiation, and wind speed in this model did not significantly change the quality of the regression. This further supports the moisture limitation of the system.

4 Discussion

4.1 Energy balance

The most striking observation is that the savanna-forest had consistently higher levels of both sensible and latent heat flux across all months (figure 9). Sensible heat fluxes over the two surfaces showed the greatest difference in November and

5   March. Latent heat flux is the most different between the two land uses in August and May, transition times when the access to water in the catchment is not uniform. The greatest similarity between the two land covers was during the wet season, May through September. The difference between the energy balance of the two sites was the most accentuated in the transition from the wet to dry season that occurred in the month of October for sensible heat flux and in the early wet season for latent energy flux (figure 8). These times of year are when we expect land use changes to have the most impact. The net

10   radiation was very similar over both land surfaces for the transition from dry to wet that occurred in May. The remainder of the energy budget showed fewer clear patterns, but across seasons, it was greater over the field, likely due to larger ground heat flux into the bare soil.

Two contrasting trends explain why the sensible heat fluxes becomes less similar as the year progresses whereas the latent heat fluxes becomes more similar. First, at the start of the year, the agricultural field is covered with bare ground and the

15   rocks are exposed above the forested area, and throughout the growing season, the bare ground is progressively covered with grass whereas on the hill, the rocks remains exposed. At the end of the dry season, the grass senesces and remains until it is burned in late December or January. The contrast of the annual cycles of bare ground and bare rock drives the difference in sensible heat flux. Second, at the start of the year, the upper trees have access to water coming from the springs at the base of the rocks. Although the level of water availability and vegetation increases during the wet season and declines during the

20   following dry season, it is permanent. In contrast, the water availability and the corresponding greenness completely follow the annual cycle of precipitation, driving the variation in latent heat. The ephemeral stream stops flowing at the end of December, when the grasses dry up and the latent heat returns to being drastically different between the two sites.

Our observations of H and L_eE are higher than fluxes previously measured in the region (Bagayoko et al., 2007; Dolman et al., 1997; Gash et al., 1997; Guichard et al., 2009; Guyot et al., 2009; Mauder et al., 2006; Schüttemeyer et al., 2006; Timouk

25   et al., 2009), which can be explained by its location inside a semi-protected area with regionally relative high amount of vegetation, increasing L_eE, and an abundance of rocks, raising H. This is consistent with local land management philosophy, which emphasizes the importance of maintaining the gallery forest, and springs therein, as a common moisture reservoir in the dry season and in case of drought. More continuous, long-term measurements during extreme years would prove the validity of this local belief. It also makes clear that the forest, even though it is primarily an open wooded savanna, has a

30   higher level of productivity than the rain-fed hand-farmed fields.

Our values of sensible and latent heat flux are most similar to those measured in Ejura, Ghana in 2002 (Schüttemeyer et al., 2006). Ejura is about 500 km from our site, and though quite far and typically placed in a different category of climate, we measure similar values compared to other areas of West Africa (Guyot et al., 2009), perhaps because measurements took

11

Hydrology and
Earth System
Sciences
Discussions
Open Access
EGU

place in November, when vegetation would be most similar to that at our site. Kompienga is the most similar and closest to ours, though overlapping in terms of seasons, but measurements are still lower than ours (Bagayoko et al., 2007). This might be explained by Tambarga-Madjoari's location in the midst of a natural park and hunting concession as well as our measurement of a gallery forest, which would demonstrate the importance of the nearby vegetation cover. On the whole, our

5   measurements are comparable to those elsewhere in West Africa, given that most of these sites (Mali, Niger) are more sahelian, and thus have less moisture availability, and others (Nigeria, Benin, Ghana) are considerably further south and thus have denser vegetation (White, 1986). The scale incongruity between the turbulent flux (sensible and latent) flux measurements and the net radiation may explain our lack of closure, instead of, for example surface heat water storage during floods (Guyot et al., 2009).

10   **4.2 Evaporative Fraction**

We can compare our values of evaporative fraction with other environmental conditions. Over West Africa, the self-preservation concept of the evaporative fraction could be used together with variables such as albedo, temperature at the surface, and a vegetation index to obtain a reasonable estimate of evaporation (Compaore, 2006). A high correlation between mid-day evaporation and the evaporative fraction exists in Kenyan grasslands (Farah et al., 2004). Evaporative fraction

15   might be affected by cloud cover which alters incoming radiation (Brutsaert and Sugita, 1992), however cloudiness is not related to the stability of evaporative fraction in 2005-2006 in Brazil (Santos et al., 2010). Evaporative fraction may also be related to other environmental parameters that are increasingly available and reliable which are obtained remotely through satellites, such as soil moisture (Crago, 1996; Hall et al., 1992).

4.3 Social Context

20   The gallery forest over which we measure fluxes includes two springs that were the main water source for the village at its founding until a generation ago (Ceperley, 2014). Its important role in local history means that special institutions existed in local tradition for its conservation. For example, wetlands, and other areas with abundant water, fall into a gourmantche category for land called "Tinjali" or land that was not farmed because of cultural taboos until recent development projects and the introduction of rice farming (Swanson, 1978). In addition, since it is forested, it is protected because gourmantche

25   believe that trees have spirits, which may prohibit them from being cut or used, and that some are considered good and some bad. So it is reasonable to conclude that the presence of the forest is not only because the water availability provides the habitat, but also because the village has protected on some level. Additionally, it is reasonable to think that the institutions that protect this forest are not only protecting it, but also the ecosystem services that it preserves. Our work suggests that these ecosystem services include the cycling of moisture into the atmosphere and the eventual generation of rainfall. In this

30   light, gourmantche myth explains that there is a sack of water above the atmosphere that spirits can pierce, bringing rain delivered by clouds (Alves, 2012). If the gods pierced those clouds with "trees" then our research seems to be right on target

Hydrology and
Earth System
Sciences

Open Access

EGU

Discussions

in terms of validating what traditions have long known. This is an important tool, as land use becomes more and more contested, the validation of local institutions or land uses can ensure the continuation of these practices.

5 Conclusions

Sensible and latent heat fluxes were higher over a savanna-forest than a semi-cultivated (millet-fallow) field according to our
5 measurements in a sudanian ecosystem of West Africa in 2009 and 2010. The sensible heat and latent energy are generally higher over the savanna-forest because of its more permanent water availability and corresponding greenness, higher productivity and the amount of rocky terrain. For example, the diurnal cycle of latent energy peaked earlier in the day during the dry season, suggesting depletion of all available moisture by late morning. These observations of sensible and latent heat flux are higher than fluxes previously measured in the region, potentially due to this site's location inside of a semi-protected
10 area. Analysis of wind sectors separately revealed that particular sectors, corresponding to the location of particular features, for example over the ephemeral wetland and the gallery forest, contributed higher amounts to the flux. Local land management emphasizes the importance of maintaining the gallery forest, and springs therein, as a common humidity reservoir in the dry season and in case of drought. Changes in land cover may even have consequences for local rainfall triggering, causing cascading effects that transform both the energy and water budgets.

15 Continuous, long-term measurements during drought and moist years are essential to prove the long-term validity of our observations. Additionally, variations in exchanges according to small landscape features could result in enormous underestimation for up-scaling. We recommend using eddy-covariance measurements such as these to improve estimates with more easily maintained and obtained meteorological station and satellite data. The evaporative fraction is dependent on NDVI, which is an important finding for modeling and up-scaling. Efforts focused on preserving hydrologic services need to
20 take anomalies into account and reinforce cultural institutions that protect wetlands and gallery forests.

The development of a simple NDVI based indicator of evaporative fraction is transferable to other semi-arid systems, agroforestry parklands, and open wooded savannas around the globe. Globally, the African continent and often semi-arid environments represent a gap in observations of land atmosphere interactions. This study is an important step in filling this gap and proposing a tool with still greater potential.

6 Acknowledgements

References

5 Abiodun, B. J., Pal, J. S., Afiesimama, E. A., Gutowski, W. J. and Adedoyin, A.: Simulation of West African monsoon using RegCM3 Part II: impacts of deforestation and desertification, Theor. Appl. Climatol., 93, 245–261, 2008.

Alves, J. P. G.: Anthropologie et écosystèmes au Niger: humains, lions et esprits de la forêt dans la culture gourmantché., 2012.

Arbonnier, M.: Trees, Shrubs and lianas of West African dry Zones, CIRAD, MNHN., 2004.

10 Aubinet, M., Feigenwinter, C., Heinesch, B., Laffineur, Q., Papale, D., Reichstein, M., Rinne, J. and Gorsel, E. V.: Nighttime Flux Correction, in Eddy Covariance, edited by M. Aubinet, T. Vesala, and D. Papale, pp. 133–157, Springer Netherlands., 2012.

Bagayoko, F., Yonkeu, S., Elbers, J. and van de Giesen, N.: Energy partitioning over the West African savanna: Multi-year evaporation and surface conductance measurements in Eastern Burkina Faso, J. Hydrol., 334(3–4), 545–559, 15 doi:10.1016/j.jhydrol.2006.10.035, 2007.

Bateni, S. M. and Entekhabi, D.: Relative efficiency of land surface energy balance components, Water Resour. Res., 48(W04510), 2012.

Bordes, C.: La Gestion Des Arbres Par Les Paysans: Etude d'une enclave au milieu de reserves forestieres au sud-est du Burkina Faso, Ingenieur, ISTOM., 2010.

20 Brutsaert, W.: Evaporation into the Atmosphere: Theory, History, and Applications, Kluwer Academic Publishers, Dordrecht, The Netherlands., 1982.

Brutsaert, W. and Parlange, M. B.: The Unstable Surface Layer Above the Forest: Regional Evaporation and Heat Flux, Water Resour. Res., 28(12), 3129–3134, 1992.

Brutsaert, W. and Sugita, M.: Application of Self-Preservation in the Diurnal Evolution of the Surface Energy Budget to 25 Determine Daily Evaporation, J. Geophys. Res., 97(D17), 18377–18382, 1992.

Burba, G.: Eddy Covariance Method for Scientific, Industrial, Agricultural and Regulatory Applications, Li-COR Biosciences., 2005.

Burba, G.: Eddy Covariance Method for Scientific, Industrial, Agricultural and Regulatory Applications: A Field Book on Measuring Ecosystem Gas Exchange and Areal Emission Rates, LI-Cor Biosciences., 2013.

30 Ceperley, N. C.: Ecohydrology of a Mixed Savanna-Agricultural Catchment in South-East Burkina Faso, West Africa, Swiss Federal Institute of Technology, Lausanne. [online] Available from: http://infoscience.epfl.ch/record/195232/files/EPFL_TH6040.pdf, 2014.

Charney, J. G.: Dynamics of deserts and drought in the Sahel, Q. J. R. Meteorol. Soc., 101(428), 193–202, 1975.

Compaore, H.: The impact of savannah vegetation on the spatial and temporal variation of the actual evapotranspiration in the Volta Basin, Navrongo, Upper East Ghana, Ecol. Dev. Ser., (36), 2006.

Crago, R. D.: Conservation and variability of the evaporative fraction during the daytime, J. Hydrol., 180(1–4), 173–194, doi:10.1016/0022-1694(95)02903-6, 1996.

Crago, R. D. and Qualls, R.: The value of intuitive concepts in evaporation research, Water Resour. Res., 49(May), n/a–n/a, doi:10.1002/wrcr.20420, 2013.

Dolman, A. J., Gash, J. H. C., Goutorbe, J.-P., Kerr, Y., Lebel, T., Prince, S. D. and Stricker, J. N. M.: The role of the land surface in Sahelian climate: HAPEX-Sahel results and future research needs, J. Hydrol., 188–189, 1067–1079, doi:10.1016/S0022-1694(96)03183-6, 1997.

Domingo, F., Serrano-Ortiz, P., Were, A., Villagarcía, L., García, M., Ramírez, D. a., Kowalski, a S., Moro, M. J., Rey, a. and Oyonarte, C.: Carbon and water exchange in semiarid ecosystems in SE Spain, J. Arid Environ., 75(12), 1271–1281, doi:10.1016/j.jaridenv.2011.06.018, 2011.

Ezzahar, J., Chehbouni, A., Hoedjes, J., Ramier, D., Boulain, N., Boubkraoui, S., Cappelaere, B., Descroix, L., Mougenot, B. and Timouk, F.: Combining scintillometer measurements and an aggregation scheme to estimate area-averaged latent heat flux during the AMMA experiment, J. Hydrol., 375(1–2), 217–226, doi:10.1016/j.jhydrol.2009.01.010, 2009.

Farah, H. O., Bastiaanssen, W. G. M. and Feddes, R. A.: Evaluation of the temporal variability of the evaporative fraction in a tropical watershed, Int. J. Appl. Earth Obs. Geoinformation, 5(2), 129–140, doi:10.1016/j.jag.2004.01.003, 2004.

Farhadi, L.: Estimation of Land Surface Water and Energy Balance Flux Components and Closure Relation Using Conditional Sampling, MIT., 2012.

Feddema, J. J., Oleson, K. W., Bonan, G. B., Mearns, L. O., Buja, L. E., Meehl, G. A. and Washington, W. M.: The importance of land-cover change in simulating future climates., Science, 310(5754), 1674–8, doi:10.1126/science.1118160, 2005.

Federer, C. a., Vörösmarty, C., Fekete, B. and Olume, V.: Sensitivity of Annual Evaporation to Soil and Root Properties in Two Models of Contrasting Complexity, J. Hydrometeorol., 4(6), 1276–1290, doi:10.1175/1525-7541(2003)004<1276:SOAETS>2.0.CO;2, 2003.

Foken, T.: The energy balance closure problem: An overview, Ecol. Appl., 18(6), 1351–1367, doi:10.1890/06-0922.1, 2008.

Foken, T., Mauder, M., Liebethal, C., Wimmer, F., Beyrich, F., Leps, J.-P., Raasch, S., DeBruin, H. A. R., Meijninger, W. M. L. and Bange, J.: Energy balance closure for the LITFASS-2003 experiment, Theor. Appl. Climatol., 101(1–2), 149–160, doi:10.1007/s00704-009-0216-8, 2009.

Foken, T., Leuning, R., Oncley, S. R., Mauder, M. and Aubinet, M.: Corrections and Data Quality Control, in Eddy Covariance: A Practical Guide to Measurement and Data Analysis, edited by M. et al Aubinet, Springer Atmospheric Sciences., 2012.

Gash, J., Kabat, P., Amadou, M., Bessemoulin, P., Billing, H., Blyth, E., Bruin, H. A. R. D., Verhoef, J. E., Friborg, T., Harrison, G., Holwill, C. J., Lloyd, C. R., Lhomme, J.-P., Moncrieff, J. B., Monteny, B. A., Puech, D., gaard, H. S., Tuzet,

A. and Verhoef, A.: The variability of evaporation during the HAPEX-Sahel intensive observation period, J. Hydrol., Hapex-Sahe(1–4), 385–3999, 1997.

Gentine, P., Entekhabi, D., Chehbouni, A., Boulet, G. and Duchemin, B.: Analysis of evaporative fraction diurnal behavior, Agric. For. Meteorol., 143, 13–29, 2007.

5 Guichard, F., Kergoat, L., Mougin, E., Timouk, F., Baup, F., Hiernaux, P. and Lavenu, F.: Surface thermodynamics and radiative budget in the Sahelian Gourma: Seasonal and diurnal cycles, J. Hydrol., 375(1–2), 161–177, doi:10.1016/j.jhydrol.2008.09.007, 2009.

Guo, Z., Dirmeyer, P. A., Koster, R. D., Bonan, G., Edmond Chan, D., Cox, P., Gordon, C. T., Kanae, S., Kowalczyk, E., Lawrence, D., Liu, I., Cheng-Hsu, Lu, A., Malyshev, S., McAvaney, B., McGregor, J. L., Mitchell, K., Mocko, D., Oki, T.,
10 Keith, W., Oleson, C., Pitman, A., Sud, Y. C., Taylor, C. M., Verseghy, D., Vasic, R., Xue, Y. and Yamada, T.: GLACE : The Global Land – Atmosphere Coupling Experiment. Part II : Analysis, Am. Meteorlogical Soc., 7, 611–625, 2006.

Guyot, A., Cohard, J.-M., Anquetin, S., Galle, S. and Lloyd, C. R.: Combined analysis of energy and water balances to estimate latent heat flux of a sudanian small catchment, J. Hydrol., 375(1–2), 227–240, doi:10.1016/j.jhydrol.2008.12.027, 2009.

15 Hall, F. G., Huemmrich, K. F., Goetz, S. J., Sellers, P. J. and Nickeson, J. E.: Satellite Remote Sensing of Surface Energy Balance: Success, Failures, and Unresolved Issues in FIFE, J. Geophys. Res., 97(D17), 19061–19089, 1992.

Higgins, C. W.: A-posteriori analysis of surface energy budget closure to determine missed energy pathways, Geophys. Res. Lett., 39(19), 1–5, doi:10.1029/2012GL052918, 2012.

Ingelrest, F., Barrenetxea, G., Schaefer, G., Vetterli, M., Couach, O. and Parlange, M.: SensorScope, ACM Trans. Sens.
20 Netw., 6(2), 1–32, doi:10.1145/1689239.1689247, 2010.

Katul, G. G. and Parlange, M. B.: A Penman-Brutsaert Model for Wet Surface Evaporation, Water Resour. Res., 28(1), 121–126, 1992.

Krishnan, P., Meyers, T. P., Scott, R. L., Kennedy, L. and Heuer, M.: Energy exchange and evapotranspiration over two temperate semi-arid grasslands in North America, Agric. For. Meteorol., 153, 31–44, doi:10.1016/j.agrformet.2011.09.017,
25 2012.

Kustas, W. P., Rango, A. and Uijlenhoet, R.: A simple energy budget algorithm for the snowmelt runoff model, Water Resour. Res., 30(5), 1515–1527, doi:10.1029/94WR00152, 1994.

Leuning, R.: The correct form of the Webb, Pearman and Leuning equation for eddy fluxes of trace gases in steady and non-steady state, horizontally homogeneous flows, Bound.-Layer Meteorol., 123(2), 263–267, 2007.

30 Lhomme, J.-P. and Elguero, E.: Examination of evaporative fraction diurnal behaviour using a soil-vegetation model coupled with a mixed-layer model, Hydrol. Earth Syst. Sci., 9(2), 259–270, 1999.

Mande, T., Ceperley, N., Barrenetxea, G., Repetti, A. and Niang, D.: Rainfall-Runoff Processes in a Mixed Sudanian Savanna Agriculture Catchment : Use of a distributed sensor network, in Geophysical Research Abstracts, vol. 13, p. 1, Vienna, Austria, 2011.

Mauder, M., Jegede, O. O., Okogbue, E. C., Wimmer, F. and Foken, T.: Surface energy balance measurements at a tropical site in West Africa during the transition from dry to wet season, Theor. Appl. Climatol., 89(3–4), 171–183, doi:10.1007/s00704-006-0252-6, 2006.

5 Nadeau, D. F., Brutsaert, W., Parlange, M. B., Bou-Zeid, E., Barrenetxea, G., Couach, O., Boldi, M.-O., Selker, J. S. and Vetterli, M.: Estimation of urban sensible heat flux using a dense wireless network of observations, Environ. Fluid Mech., 9(6), 635–653, doi:10.1007/s10652-009-9150-7, 2009.

Nicholson, S. E., Tucker, C. J. and Ba, M. B.: Desertification, drought, and surface vegetation: An example from the West African Sahel, Bull. Am. Meteorol. Soc., 79(5), 815–830, 1998.

Oldroyd, H. J., Pardyjak, E. R., Huwald, H. and Parlange, M. B.: Adapting Tilt Corrections and the Governing Flow
10 Equations for Steep, Fully Three-Dimensional, Mountainous Terrain, Bound.-Layer Meteorol., 1–27, 2015.

Parlange, M. B. and Katul, G. G.: Estimation of the diurnal variation of potential evaporation from a wet bare soil surface, J. Hydrol., 132(1–4), 71–89, doi:10.1016/0022-1694(92)90173-S, 1992.

Pielke, R. A., Marland, G., Betts, R. A., Chase, T. N., Eastman, J. L., Niles, J. O., Niyogi, D. D. S. and Running, S. W.: The influence of land-use change and landscape dynamics on the climate system: relevance to climate-change policy beyond the
15 radiative effect of greenhouse gases., Philos. Transact. A Math. Phys. Eng. Sci., 360(1797), 1705–1719, 2002.

Porte-Agel, F., Parlange, M. B., Cahill, A. T., Gruber, A. and Porte, F.: Mixture of Time Scales in Evaporation : Desorption and Self-Similarity of Energy Fluxes, Agron. J., 92(September-October), 832–836, 2000.

Rebmann, C., Kolle, O., Heinesch, B., Queck, R., Ibrom, A. and Aubinet, M.: Data Acquisition and Flux Calculations, in Eddy Covariance, edited by M. Aubinet, T. Vesala, and D. Papale, pp. 59–83, Springer Netherlands., 2012.

20 Santos, C. A. C. D., Silva, B. B. D. and Rao, T. V. R.: Analysis of the evaporative fraction using eddy covariance and remote sensing techniques, Rev. Bras. Meteorol., 25(4), 427–436, doi:10.1590/S0102-77862010000400002, 2010.

Schüttemeyer, D., Moene, A. F., Holtslag, A. A. M., Bruin, H. A. R. and van de Giesen, N.: Surface Fluxes and Characteristics of Drying Semi-Arid Terrain in West Africa, Bound.-Layer Meteorol., 118(3), 583–612, doi:10.1007/s10546-005-9028-2, 2006.

25 Shuttleworth, W. J.: FIFE: the variation in energy partition at surface flux sites, Remote Sens. Large-Scale Glob. Process. IAHS Publ., (186), 1989.

Simoni, S., Padoan, S., Nadeau, D. F., Diebold, M., Porporato, A., Barrenetxea, G., Ingelrest, F., Vetterli, M. and Parlange, M. B.: Hydrologic response of an alpine watershed: Application of a meteorological wireless sensor network to understand streamflow generation, Water Resour. Res., 47(10), doi:10.1029/2011WR010730, 2011.

30 Steiner, A. L., Pal, J. S., Rauscher, S. A., Bell, J. L., Diffenbaugh, N. S., Boone, A., Sloan, L. C. and Giorgi, F.: Land surface coupling in regional climate simulations of the West African monsoon, Clim. Dyn., 33(869–892), 2009.

Swanson, R. A.: Gourmantche agriculture, Ouagadougou USAID, 1978.

Swets, D. L., Reed, B. C., Rowland, J. D. and Marko, S. E.: A weighted least-squares approach to temporal NDVI smoothing, in Proceedings of the 1999 ASPRS Annual Conference, Portland, Oregon, 1999.

Sylla, M. B., Pal, J. S. and Wang, G.: Impact of land cover characterization on regional climate modelling over West Africa, Clim. Dyn., 2015.

Szilagyi, J. and Parlange, M. B.: Defining Watershed-Scale Evaporation Using a Normalized Difference Vegetation Index, J. Am. Water Resour. Assoc., 35(5), 1245–1255, doi:10.1111/j.1752-1688.1999.tb04211.x, 1999.

5   Szilagyi, J., Rundquist, D. C., Gosselin, D. C. and Parlange, M. B.: NDVI relationship to monthly evaporation, Geophys. Res. Lett., 25(10), 1753–1756, 1998.

Timouk, F., Kergoat, L., Mougin, E., Lloyd, C. R., Ceschia, E., Cohard, J.-M., Rosnay, P., Hiernaux, P., Demarez, V. and Taylor, C. M.: Response of surface energy balance to water regime and vegetation development in a Sahelian landscape, J. Hydrol., 1–43, 2009.

10   Topp, G. C., Davis, J. L. and Annan, A. P.: Electromagnetic determination of soil water content: Measurements in coaxial transmission lines, Water Resour. Res., 16(3), 574–582, doi:10.1029/WR016i003p00574, 1980.

Vitousek, P. M.: Human Domination of Earth's Ecosystems, Science, 277(5325), 494–499, doi:10.1126/science.277.5325.494, 1997.

Webb, E., Pearman, G. and Leuning, R.: Correction of flux measurements for density effects due to heat and water vapour
15   transfer, Q. J. R. Meteorol. Soc., 106(447), 85–100, 1980.

White, F.: la vegetation de l'Afrique: Memoire accompagnant la carte de vegetation de l'Afrique., 1986.

Whiteman, C. D. and Allwine, K. J.: Extraterrestrial solar radiation on inclined surfaces, Environ. Softw., 1(3), 164–169, 1986.

Wilczak, J. M., Oncley, S. P. and Stage, S. A.: Sonic anemometer tilt correction algorithms, Bound.-Layer Meteorol., 99(1),
20   127–150, 2001.

Williams, C. A., Reichstein, M., Buchmann, N., Baldocchi, D., Beer, C., Schwalm, C., Wohlfahrt, G., Hasler, N., Bernhofer, C., Foken, T., Papale, D., Schymanski, S. and Schaefer, K.: Climate and vegetation controls on the surface water balance: Synthesis of evapotranspiration measured across a global network of flux towers, Water Resour. Res., 48(6), W06523, doi:10.1029/2011WR011586, 2012.
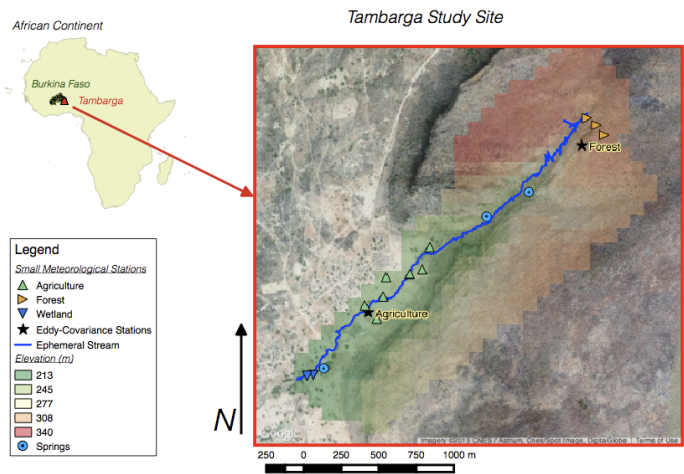
Figure 1: Map of Study Site. The site is located next to the village of Tambarga, in the southeastern corner of Burkina Faso, a
land-locked country in West Africa. There is an ephemeral stream that runs through the village, shown in blue, 100 m of elevation
change between the agricultural fields and the plateau, as shown with the topographic shadings, and three springs shown as blue
circles. Meteorological stations are visible as triangles, coloured by land use (orange for forest, green for agriculture, and blue for
wetland), and the two eddy-covariance stations are visible as black stars. The village of Tambarga is visible in the satellite image,
in the centre of the map.

Instrument	Measurement	Height/Depth	Number	Interval	Time Span
CSAT-3 Sonic Anemometer (Campbell Scientific, Logan, UT, USA)	3D Wind Speed and Direction, Air Temperature	2.2 m	3	20 Hz, proc. 30 min.	May 2009 - October 2010
Li- 7500 Infrared Gas Analyser (LICOR, Lincoln, NE, USA)	H_2O Concentration	2.2 m	3	20 Hz, proc. 30 min.	May 2009 - October 2010
CNR2 Radiometer (Kipp & Zonen, Delft, The Netherlands)	SW LW Radiation	2.1 m	2	1 min.	October 2009 - October 2010
HMP450 (Campbell Scientific, Logan, UT, USA) with Radiation Shield	Air Temperature, Air Humidity	2.25 m	2	1 min.	May 2009 - October 2010
Pluviometer 3029	Precipitation	1 m	1	0.1 mm	May 2009 -

19

(Précis Mécanique, Bezons, Cedex, France)					January 2015
Davis Instruments (Hayward, CA, USA)	Precipitation	.02 m	12	1 min.	May 2009 - January 2015
Davis Instruments (Hayward, CA, USA)	Shortwave Solar Radiation, Incoming	1.8m	12	1 min.	May 2009 - January 2015
Infrared thermometer TN901 (Zytemp, Taiwan, R.O.C.)	Surface Temperature	1.1 m	12	1 min.	May 2009 - January 2015
SHT7 (Sensiron AG, Staefa ZH, Switzerland)	Air Temperature & Humidity	1.7 m	12	1 min.	May 2009 - January 2015
5TM, 5TE, ECTM (Decagon, Pullman, WA, USA)	Soil Humidity	5-30 cm	~ 24 (varied)	1 min.	May 2009 - January 2015

Table 1: Inventory of Instruments used for Energy Balance Analysis: The name of the sensor or instrument is followed by the measurement it performs, the height and depth of each sensor, the total number used, and the interval of measurement.

5
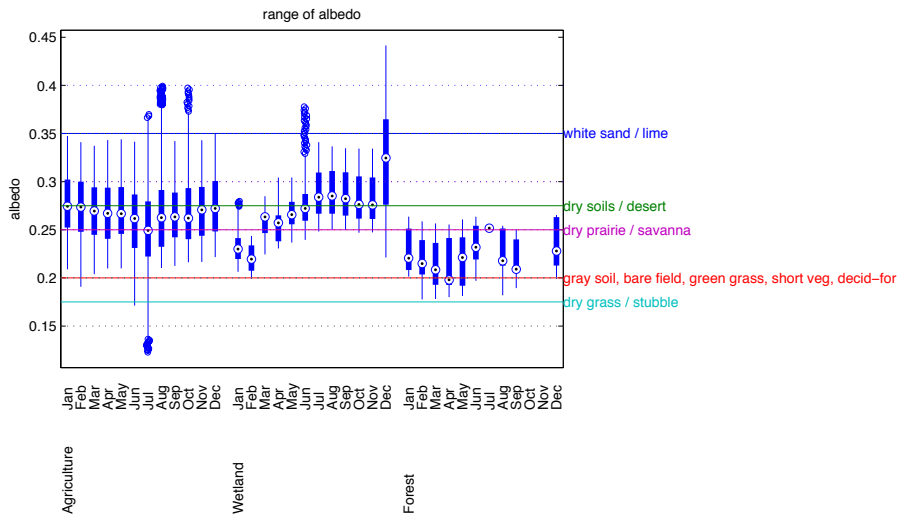
Figure 2: Distribution of albedo by landcover (Agricultural, Wetland, and Forest) and by month for the study period. The central dot is the median, the edges of the box are the 25th and 75th percentiles, the whiskers extend to the most extreme data points not considered outliers, and outliers are plotted individually. Average values for various land-covers listed by Brutsaert (1982) are drawn and labelled to the right. Ranges for these are shown in dotted lines. Our values mostly range between those of bare field or
5 **green grass and dry soils and desert, with dry prairie or savanna making a good mid value.**
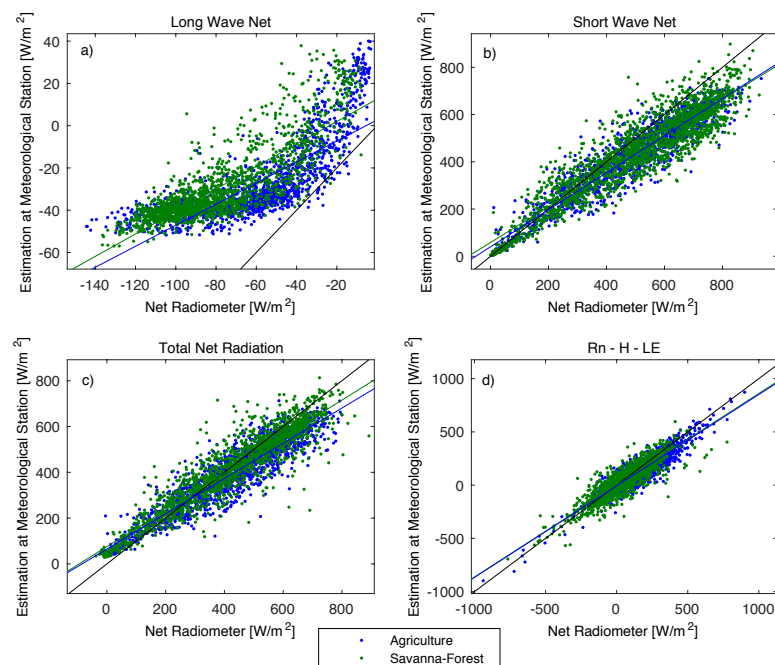
	Agriculture	Savanna-Forest
a) LW_{net}	0.58	0.50
b) SW_{net}	0.76	0.78
c) R_n	0.80	0.77
R_n-H- L_eE	0.86	0.86

Figure 3: Comparison of measurements and calculations on a half hour scale of (a) net short wave, (b) net long wave, and (c) total radiation and the residual (not shown, correlation in table) after subtracting the measured turbulent fluxes. In all cases the slope is
10 **less than 1, which means that the measurements are greater than the calculation. The slopes of the regression lines are in the accompanying table. In each plot, measurements over the agricultural field are shown in blue and over the savanna-forest are shown in green. Black lines show the one to one line and coloured lines show the least squared regression lines.**
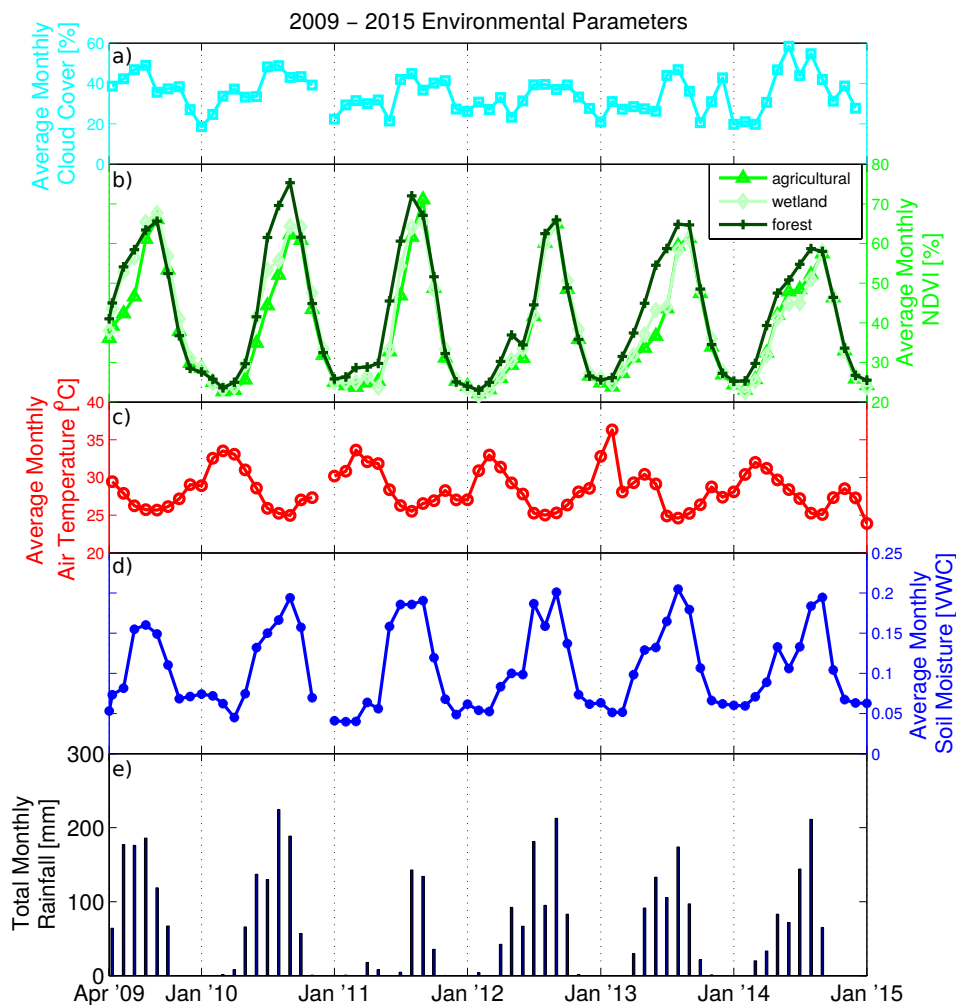
Figure 4: Environmental Parameters at Study Site for Monitoring Period (2009 - 2015): a) Cloud cover measured with shortwave radiometers and averaged over all stations; b) Average NDVI from MODIS satellite data (250 meter resolution, 10-day composite) averaged over each landcover of pixels containing stations; c) Monthly average air temperature (red line), also averaged for all stations; d) Volumetric soil moisture averaged over all stations and all land covers between 5 and 30 cm depth (blue line); And e) monthly rainfall (missing bars indicate lack of rain). Note the strong seasonality of all variables.

Hydrology and
Earth System
Sciences
Open Access
Discussions
EGU
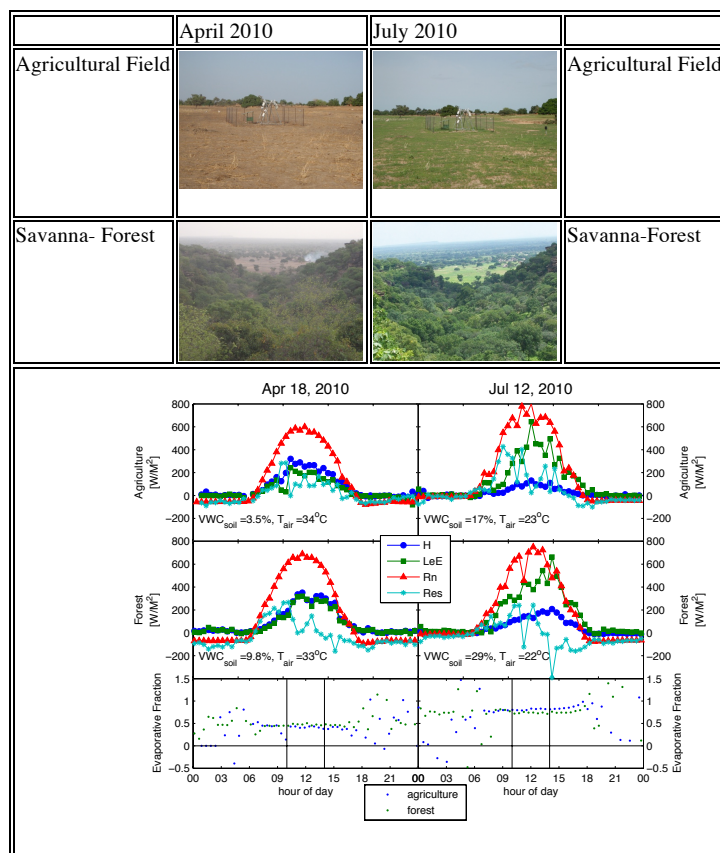
Figure 5: Diurnal Cycle of the Energy Balance. The upper four photographs correspond to the four subplots - the date of the photograph is the same month as the representative plot of diurnal energy budget. Note that April (left) is the dry season and the atmosphere was very hazy, in part due to fires. July is the start of the rainy or wet season (right). The energy budget is made up of the sensible heat (H, blue), latent heat (LeE, green), net radiation (R_n, red) on the y-axis (W/m2) over the savanna-forest (middle row) and agricultural land (top row) according to time of day (x-axis, 24 hours). The residual of the energy budget is also shown in turquoise. The final row shows the half hour calculation of evaporative fraction. Daily averages were taken between 10 and 14 hours, shown with the vertical lines, with the savanna-forest in green and agriculture in blue.
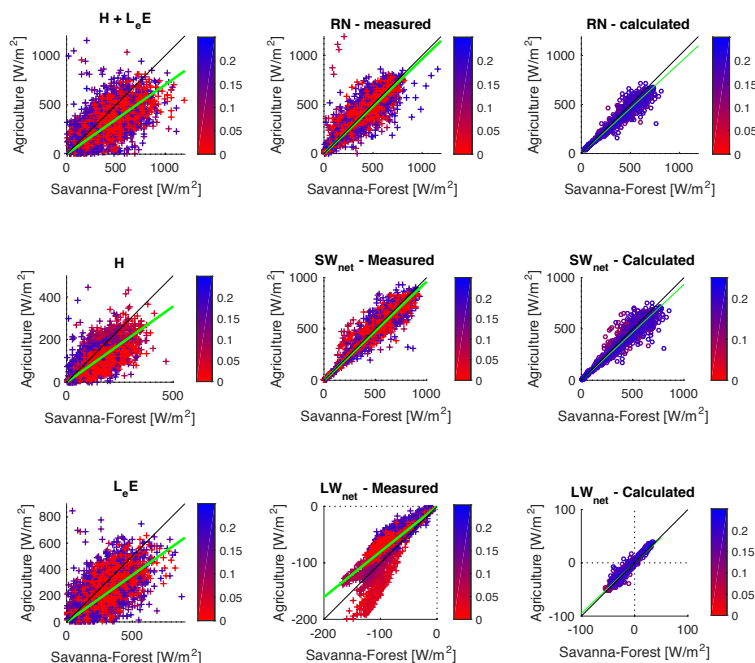
Figure 6: Comparison between fluxes measured over the savanna-forest and the field. In each plot, colour indicates soil volumetric water content, red is dry and blue is wet. The least square regression lines are shown in green and the 1:1 lines are in black. Measurements over the savanna-forest are on the x-axis and those over agriculture are on the y-axis. All fits were significant (p<0.005). The middle column shows the components of net radiation calculated with the net radiometers. The right shows the components of net radiation calculated using parameters measured at the small meteorological stations: Ta, incoming SW, Ts, etc. There is less difference between the savanna-forest and the field when net long wave is calculated. The top left plot shows the total available energy (H+ L_eE); the top right shows net radiation; the middle right two plots show long and short wave net radiation, respectively; and the bottom left two show separate H and L_eE respectively. The fluxes (daytime, half-hour time step) measured over the field were consistently lower than those measured over the savanna-forest.
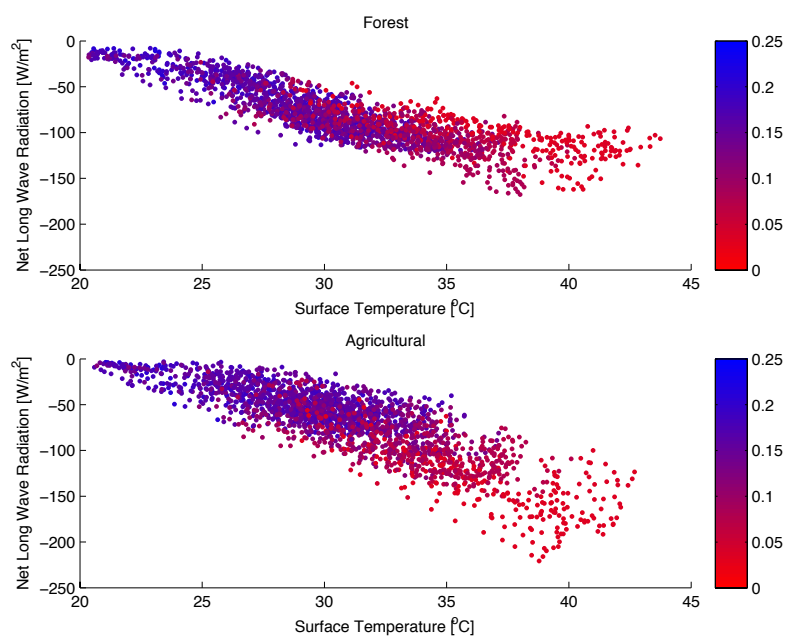
Figure 7: Net Long-wave Radiation Response to Soil Moisture and Surface Temperature. Surface temperature and net long wave radiation had a strong negative correlation with each other and also with volumetric soil water content, shown by the colour. The pattern of this correlation varied by land cover, savanna-forest above and agriculture below.
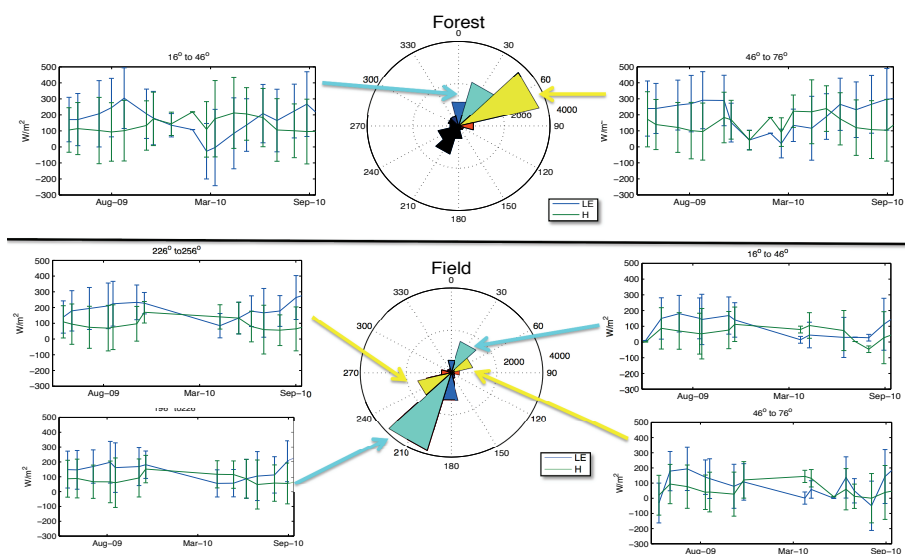
Figure 8: Two dominant wind sectors for each eddy-covariance set up are plotted: Above the two over the savanna field and below the 4 over the agricultural field. Mean latent energy for each month with standard deviations is shown in blue and sensible heat in green. Note that for some months, there was no data. We see that each sector has a distinct signature of when latent energy flux is greater than sensible heat flux.

Hydrology and
Earth System
Sciences
Discussions

Open Access

EGU
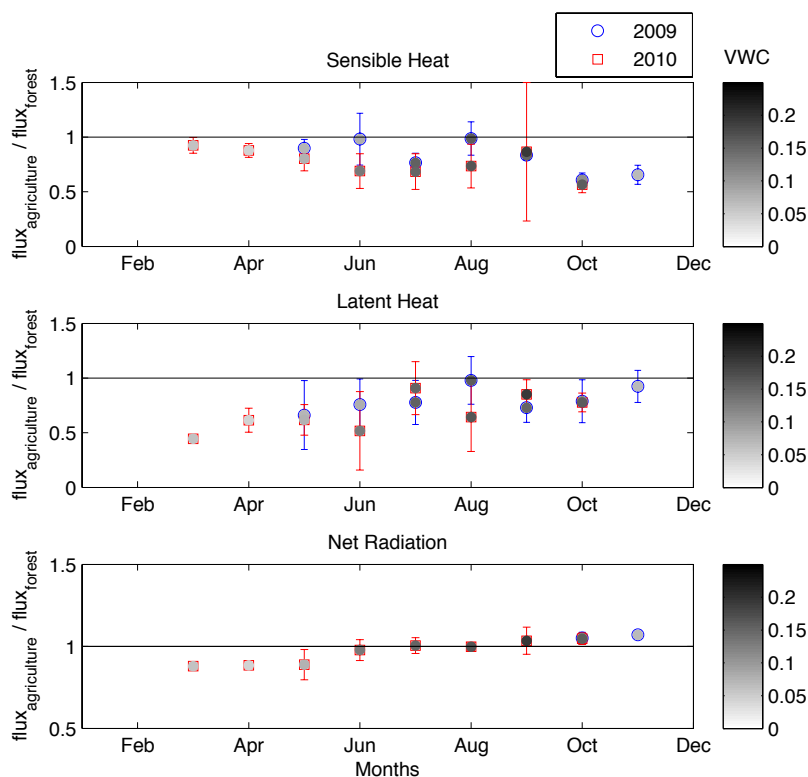
Figure 9: Examination of ratio of the daily fluxes by month and year. The ratios between flux measurements over the field and savanna-forest is shown according to month (x - axis) and year (in colour: blue is 2009 and red is 2010). The soil moisture value is shown with shading. Error bars show the standard deviation around the average of daily ratios. Points below the 1 line indicate when the savanna-forest flux is higher than the agricultural field flux. It is important to note that the field was farmed in 2009 until the end of July but left fallow in 2010.
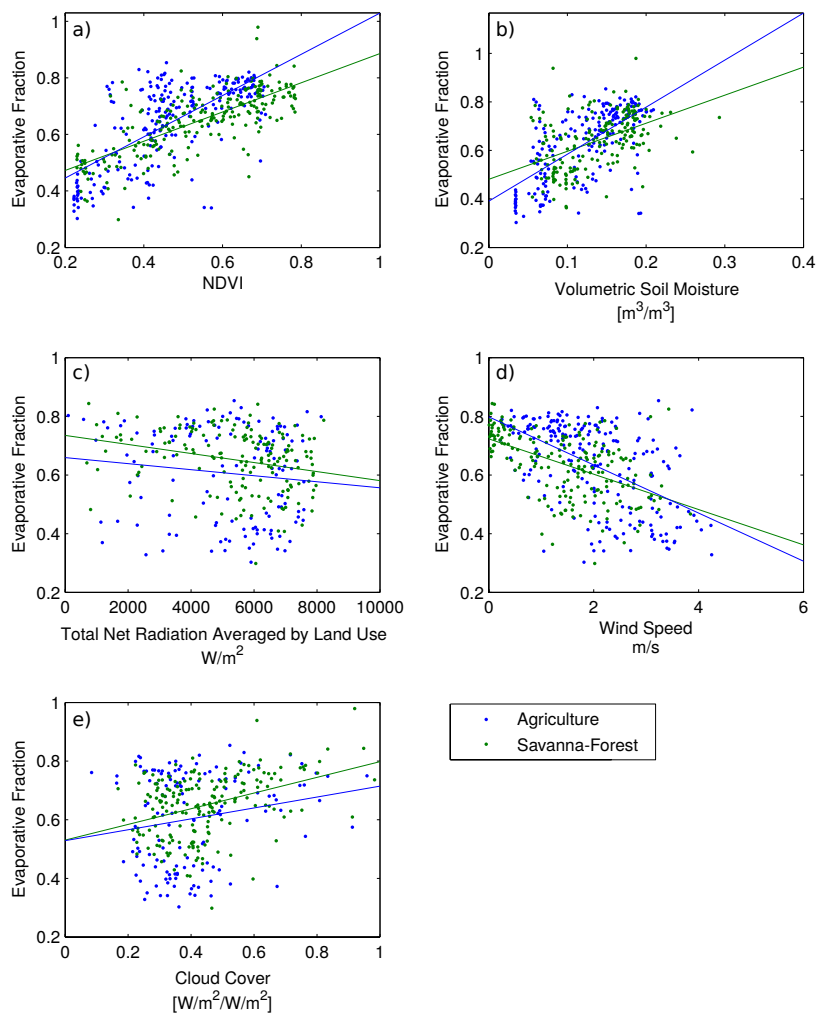
Figure 10: Daily evaporative fraction over study period for the agricultural field (blue) and the savanna-forest (green) compared with the observed a) NDVI, b) VWC, c) wind speed, d) net radiation, and e) cloud cover. In all cases, environmental variables are from the average of stations with the same landcover with the energy balance station. These plots show a better correlation with NDVI and VWC (top row), suggesting moisture, not radiation, limited system. The least squared regression lines are shown for each plot.

28

Figure 11: Further Examination of relationship between Soil Moisture, Vegetation Index, and Evaporative Fraction. Upper plots show results of linear regression model relating soil volumetric water content (y-axis), vegetation index (x-axis), and evaporative fraction (colour) over agriculture (left) and over savanna-forest (right). Data points are plotted in black. Second row shows the quality of fit between the measured evaporative fraction and the linear regression model of evaporative fraction. The 1:1 line is in red and the 95% confidence interval is shown with dotted lines for the range of available soil and vegetation measurements over agriculture (left) and savanna-forest (right). The details of the regression are shown in the table with quality of fit for agriculture (above) and savanna-forest (below).
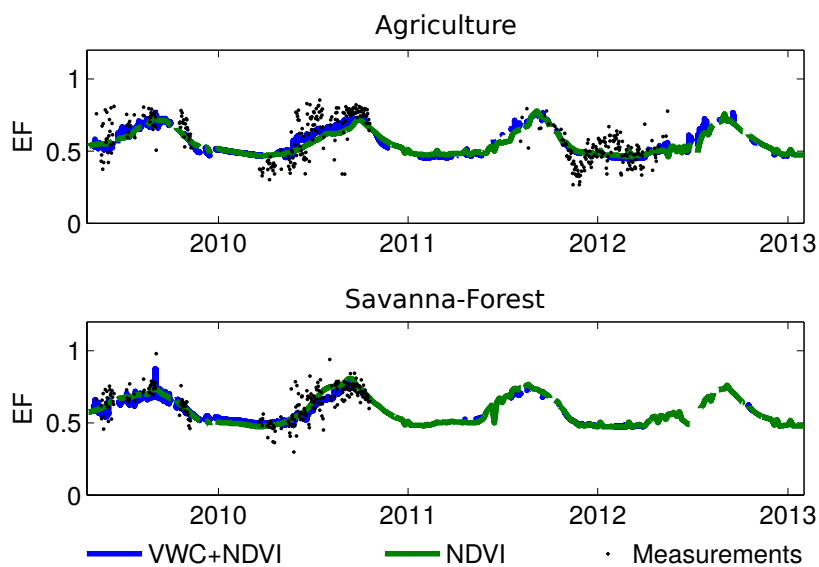
29

Figure 12: Time series of evaporative fraction. Upper plot shows evaporative fraction over the field and lower plot shows
evaporative fraction over the savanna-forest. Measured data points are in black (points), calculated evaporative fraction based on
soil moisture and NDVI is shown in blue and just NDVI is shown in green.